Письма в ЭЧАЯ. 2016. Т. 13, № 3(201). С. 603–610

ФИЗИКА И ТЕХНИКА УСКОРИТЕЛЕЙ

DIAGNOSTIC TECHNIQUE APPLIED FOR FEL ELECTRON BUNCHES

O. Brovko, A. Grebentsov, N. Morozov, E. Syresin [1], *M. Yurkov*

Joint Institute for Nuclear Research, Dubna

Diagnostic technique applied for FEL ultrashort electron bunches is developed by JINR–DESY collaboration in the context of the FLASH and XFEL projects. Photon diagnostics is based on calorimetric measurements and detection of undulator radiation. The infrared undulator constructed at JINR and installed at FLASH is used for longitudinal bunch shape measurements and for two-color lasing provided by the FIR and VUV undulators. The pump-probe experiments with VUV and FIR undulators provide the bunch profile measurements with resolution of several femtoseconds. Three new microchannel plate (MCP) detectors operated in X-ray range are under development now at JINR for SASE1–SASE3 of European XFEL.

Диагностическая техника, предназначенная для ультракоротких банчей, сформированных в лазерах на свободных электронах, разработана в сотрудничестве ОИЯИ–DESY при реализации проектов FLASH и XFEL. Фотонная диагностика основана на калориметрических измерениях и детектировании ондуляторного излучения. Инфракрасный ондулятор, изготовленный в ОИЯИ и установленный на FLASH, используется для измерения продольной формы электронных банчей и для двухцветной генерации излучения из инфракрасного (ИК) и ультрафиолетового (УФ) ондуляторов. Эксперименты с возбуждением и откликом для ИК- и УФ-ондуляторов обеспечивают измерения профиля банчей с разрешением несколько фемтосекунд. Три новых детектора, основанных на микроканальных пластинах и работающих в рентгеновском диапазоне, разрабатываются в настоящее время в ОИЯИ для SASE1–SASE3 европейского XFEL.

PACS: 29.20.-c; 29.25.-t

MCP DETECTOR OF EUROPEAN XFEL

An important task of the photon beam diagnostics at the European XFEL is providing reliable tools for measurements aiming at the search for fine tuning of the FEL creating SASE process (Self-Amplified Spontaneous Emission). The problem of finding SASE amplification is crucial for the XFEL because of a large synchrotron radiation background. This requires a detector with a wide dynamic range, controllable tuning to the required wavelength range, and suppression of the unwanted radiation background. The JINR–XFEL collaboration manufactured microchannel plate (MCP) based photon detectors as a primary tool for the search for fine tuning of the SASE process. Uniqueness of MCP detector permits to measure the photon pulse energy in the range of a few nJ up to 25 mJ with relative accuracy of 1%. Three MCP devices [1–4] will be installed, one after each SASE undulator of the European XFEL (SASE1, SASE2, and SASE3).

[1] E-mail: syresin@nusun.jinr.ru

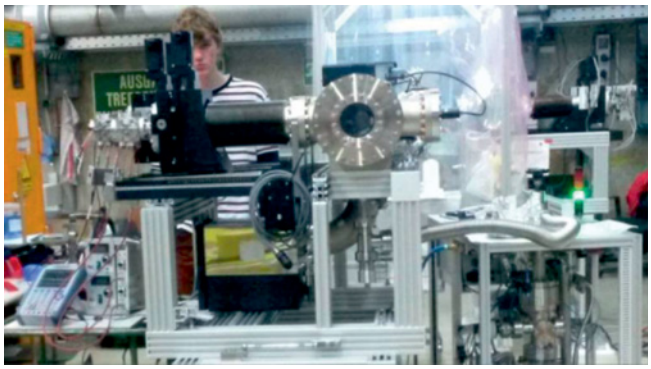

Fig. 1. XFEL SASE1 and SASE2 MCP detectors

Three different tasks can be fulfilled with the XFEL MCP-based photon detectors: study of the initial stage of the SASE regime; measurement of the photon pulse energy; and measurement of the photon beam image. The MCP detector will resolve each individual pulse at a repetition rate of 4.5 MHz. The following wavelength ranges are to be covered by three MCP stations: 0.05–0.4 nm for MCP1 and MCP2, 0.4–5 nm for MCP3.

MCP detectors for SASE1 and SASE2 (Fig. 1) are installed after the deflecting mirrors. The offset mirrors are used for two distinctive and separate purposes. Firstly, during early commissioning they cut off high harmonics of spontaneous radiation and improve the ratio of FEL/spontaneous intensity. Secondly, they are used as additional attenuators of the radiation intensity. The diamond attenuator and the Ce : YaG screen are installed in front of the first carbon coated offset mirror. The attenuation range of the mirrors combined with the diamond plate attenuators is about 10^3–10^4. The dynamic range of the MCP is 10^3–10^4.

The MCP detector for SASE1 and SASE2 [1–4] consists of a silicon photodiode, three MCPs equipped with an anode as a pulse energy monitor, and one MCP detector for imaging the photon beam. The first MCP detector port houses one silicon photodiode and two F4655 Hamamatsu MCPs, 18 mm in diameter. The PM 100-250 3D vacuum manipulator displaces these MCPs in the horizontal direction in a range of 250 mm. The range of vertical displacement is ± 2.5 cm relative to the beam axis.

The second detector port houses two MCPs: F4655 for measurement of the pulse energies and the beam observation system (BOS) MCP (model BOS-40-IDA-CH/P-47) of 40 mm diameter with a phosphor screen. The BOS MCP is set at an angle of 45° with respect to the photon beam, and a viewport allows imaging onto the charge coupled device (CCD) camera (model Basler camera GigE avA1600-50gm).

MCP detector for SASE3 [1, 2] will have an additional port with movable semitransparent mesh and wire targets for production of scattering FEL radiation similar to those used at FLASH.

The calibration of the MCP detector was realized in X-ray and UV wavelength range before installation of this detector in the XFEL tunnel. Initially the F4655 Hamamatsu MCPs were calibrated with a UV lamp. The MCP1 and MCP2 amplification gains are shown in Fig. 2. The MCP gain corresponds to 4 orders of magnitude. Previous experience from FLASH with similar F4655 Hamamatsu MCPs shows that when the light intensity is high, the applied voltage needs to be reduced, and below 1400 V the space charge effects in MCP channels start to play a significant role.

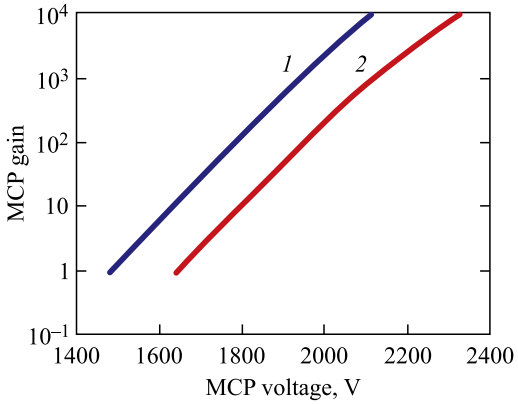

Fig. 2. Dependence of MCP1 (*1*) and MCP2 (*2*) gains on MCP voltage

Further validation tests with the MCP detector were performed at DORIS BW1 beamline. The absolute measurements of a photon pulse energy of 0.03 nJ and larger for hard X-ray radiation were performed with application of MCP and photodiode detectors.

The photon flux was in a range of $2 \cdot 10^{11}$ to $2 \cdot 10^{8}$ s^{-1}. The synchrotron radiation (SR) measurements were performed at photon energies of 8.5 to 12.4 keV. Variation of photon energy was done with the BW1 undulator gap. Vacuum pressure in the MCP-detector UHV chamber was $5 \cdot 10^{-9}$ mbar. The MCP entrance window is a 200 μm thick beryllium foil. Pulse-to-pulse photon energy measurements with MCPs and a silicon photodetector were done with 192 and 96 ns repetition intervals. The SR beam imaging measurement under X-ray irradiation was performed at test validation experiments. The X-ray beam image was measured by the MCP detector at a photon energy of 9.66 keV. The MCP beam observation system with a phosphor screen can be effectively used for search of SASE mode starting from spontaneous emission.

The gas ionization monitor (GIM) was used for measurement of the SR photon flux. Dependence of the MCP signal on the GIM signal is shown in Fig. 3. The linear behavior of the MCP1 signal versus the gas ionization monitor signal is observed at an MCP1 voltage of 1.85 kV and below.

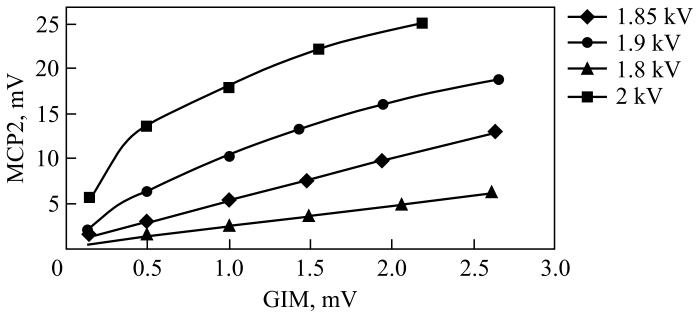

Fig. 3. Dependence of MCP2 signal on gas ionization chamber signal at different MCP2 voltages

An essential influence of secondary ions produced by X-rays in the MCP chamber at a pressure of $5 \cdot 10^{-9}$ mbar was observed during MCP operation in DORIS BW1. The nonlinear dependence of the MCP signal on X-ray beam intensity was measured at MCP voltages higher than 1.9 kV (Fig. 3). When the ion pump was switched on or off, we did not see any difference of the ion input in the MCP operation. Therefore, we assume that the X-rays produce secondary ions by ionization of residual gas atoms.

MCP gain versus photon energy of UV and X-ray radiations is given in Fig. 4 where the MCP voltage was increased from 1.8 to 1.85 kV. In accordance with the UV calibration (Fig. 4), the MCP gain corresponds to 2.1 at MCP2 voltage increase from 1.8 to 1.85 kV. For X-ray radiation at photon energy of 8.5–12.4 keV this gain varies in a range of 1.7 to 2.1.

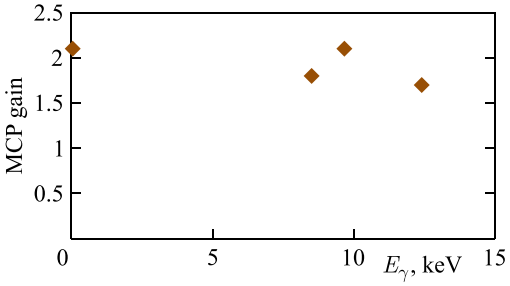

Fig. 4. Dependence of MCP2 gain on photon energy at increase of MCP voltage from 1.8 to 1.85 kV

The ratio of the MCP2 signal to SR pulse energy corresponds to 0.11–0.16 V/nJ at photon energy of 8.5–12.4 keV and MCP voltage of 1.8 kV.

The XFEL micropulse energy of 1 mJ should produce an MCP amplitude signal of 1.2 V for an MCP voltage of 1.5 kV (assuming an MCP gain reduction of 10^{-2} in comparison with 1.8 kV MCP voltage) and attenuation factor of XFEL radiation $R = 10^{-3}$ in accordance with SR test measurements of the calibration ratio 0.12 V/nJ at MCP voltage of 1.8 kV.

The SR photon flux was measured by a silicon photodiode and GIM. Linear dependence of the photodiode signal in pulsed mode versus the gas ionization monitor signal is presented in Fig. 5. Maximum photodiode current of 105 uA corresponds to SR photon flux of $2.4 \cdot 10^{11}$ s^{-1}. The ratio of photodiode signal to SR pulse energy corresponds to 0.52 V/nJ at photon energy of 9.66 keV and it is equal to 0.31 V/nJ at photon energy of 12.4 keV.

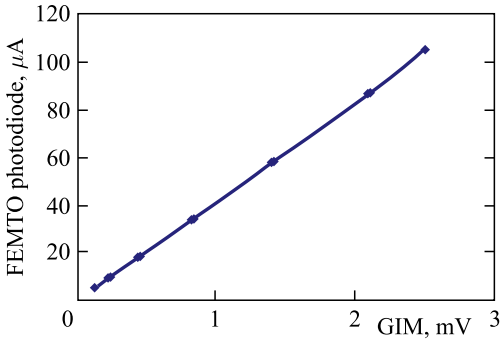

Fig. 5. Dependence of XFEL diode current on gas ionization monitor (GIM) signal at $E_\gamma = 9.66$ keV

Pulse time structures of SR with bunch repetition time of 192 and 96 ns were measured by the MCPs and photodiode detectors.

The X-ray beam image was measured by MCP detector at intensity higher than $4 \cdot 10^7$ s^{-1} at a photon energy of 9.66 keV. The MCP beam observation system with a phosphor screen is effectively used for the search of the SR photon beam position.

However, at SR tests the measured X-ray beam size at small slits of 0.2–0.4 mm was about 1.8–2 mm caused by low contrast resolution of the phosphor screen and image spot spreading. The MCP imager can be applied for search of the SASE photon beam spot; however, it cannot be used for detailed measurements of the spot shape and substructure.

JINR FAR INFRARED UNDULATOR AT FLASH

The FLASH was equipped with an infrared electromagnetic undulator (Fig. 6), tunable over a K-parameter range from 11 to 44, and producing radiation up to 200 μm at 500 MeV and up to 50 μm at 1 GeV [2, 5–9]. The purpose of the device is twofold: firstly, it is used for longitudinal electron bunch measurements; secondly, it is a powerful source of intense infrared radiation naturally synchronized to the VUV FEL pulses, as both are generated by the same electron bunches and being therefore well suited for precision pump-probe experiments.

The undulator was designed and constructed by JINR to the FLASH requirements [8]. The undulator period corresponds to 40 cm, the number of periods is 9, the magnetic field is varied in range of 0.1–1.1 T. Output undulator radiation has the following parameters: wavelength 5–200 μm, peak power 4 MW, micropulse energy 1 mJ, micropulse duration 0.5–6 ps.

The energy radiated by the far infrared (FIR) undulator is defined by the number of electrons per bunch N and a form factor $F(\lambda)$:

$$\varepsilon_{\mathrm{coh}} = \varepsilon_e \times [N + N(N-1)\,|\bar{F}(\lambda)|^2],$$

where ε_e is energy radiated by single electron. The form factor is equal to $|F(\lambda)|^2 = \exp(-2\pi\sigma/\lambda)^2$ for Gaussian bunch with r. m. s. length σ. When the wavelength is longer

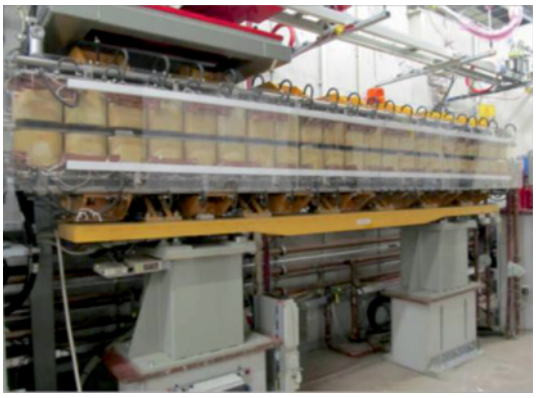

Fig. 6. FLASH far infrared undulator constructed by JINR

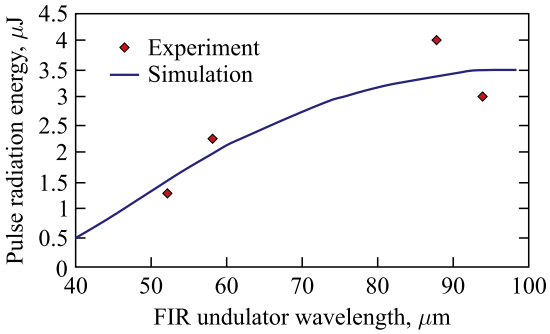

Fig. 7. Dependence of the FIR undulator pulse radiation energy on the wavelength

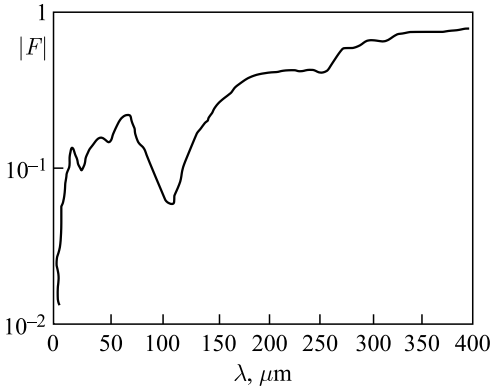

Fig. 8. Dependence of form factor on FIR radiation wavelength

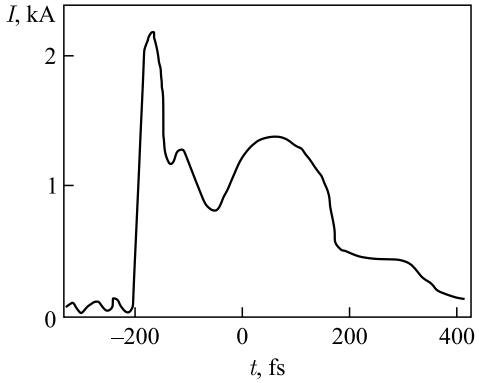

Fig. 9. Time distribution of electron current in a single-shot electron bunch reconstructed from form factor of FIR radiation

than the bunch length, the coherent radiation dominates. Measuring the spectrum in that regime one can extract the form factor and thus the charge distribution and the bunch leading spike length. The Gaussian fit (Fig. 7) corresponds to the r. m. s. leading spike length of $\sigma_{\rm ls} = 12$ μm. The r. m. s. duration of FIR pulse radiation is equal to $\tau_{\rm FIR} = \sigma_{\rm ls}/c = 40$ fs, it is a few times larger than r. m. s. pulse duration of the VUV pulse radiation.

After upgrade the detailed measurements of form factor for FIR radiation were performed (Fig. 8) [7]. The form factor permits to reconstruct the time distribution of the electron current in the electron bunch (Fig. 9) [7]. The reconstructed electron current pulse has a complicated shape with two peaks at electron energy 1.25 GeV and bunch charge 0.5 nC.

PUMP-PROBE EXPERIMENTS AT FLASH WITH JINR FIR UNDULATOR

The pump-probe experiments are very promising application of FLASH VUV and FIR undulators. The VUV and FIR undulator radiations are truly synchronized and tunable in a broad spectral range that opens new perspective for two-color pump-probe experiments at FLASH. In the first pump-probe experiments [2, 10] both FIR and VUV undulator radiations at wavelengths of 91 μm and 13.5 nm, correspondingly, passed through a krypton gas chamber. The 4-p krypton electrons are ionized in the gas chamber by the VUV photons generated during short pulse duration of 30 fs. The ionized electrons are accelerated during 3 ps in the electric field of IR light. The electron energy E_e is defined by VUV photon energy $h\omega = 91.8$ eV, the krypton electron bind energy $E_{\rm bind} = 14.1$ eV, and the vector potential of FIR electrical field $A_{\rm THz}$: $E_e = h\omega - E_{\rm bind} + evA_{\rm THz}$, here v is the electron velocity. The difference of the electron energy spectrums along and across of the vector potential $A_{\rm THz}$ direction gives the same information about the time structure of VUV radiation pulses. There is an asymmetry of the electron spectrums at small vector potentials $A_{\rm THz} \to \pm 0$ for two opposite directions of vector potential $A_{\rm THz} \to +0$ and $A_{\rm THz} \to -0$ (Fig. 10).

The effective electron energy rate $S_{\rm eff}$ is defined by equation $S_{\rm eff}^2 = S^2 \pm 4SC$, where $S = veE_{\rm THz} \cong 100$ meV/fs is the electron energy rate corresponded to FIR undulator electric

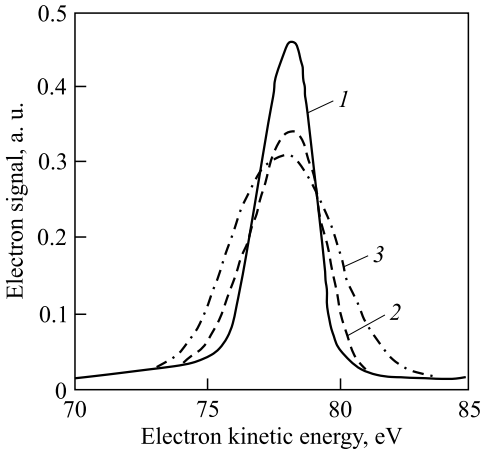

Fig. 10. Dependence of electron intensity on its kinetic energy for three different vector potentials of FIR radiation: *1* — the vector potential is perpendicular to the electron velocity, $v \perp A_{\mathrm{THz}}$; *2* — the vector potential is parallel to the electron velocity and negative, $v || A_{\mathrm{THz}}$, $A_{\mathrm{THz}} \to -0$; *3* — the vector potential is parallel to the electron velocity and positive, $v || A_{\mathrm{THz}}$, $A_{\mathrm{THz}} \to +0$

field $E_{\mathrm{THz}} = dA_{\mathrm{eff}}/dt$, $C = hd\omega/dt \cong (5 \pm 7)$ meV/fs is the VUV photon energy chirp related to the beam electron energy chirp produced in FEL lasing spike at bunch compression. The sign $\pm$ corresponds to cases of the vector potential $A_{\mathrm{THz}} \to \pm 0$. The r. m. s. VUV radiation pulse duration is equal to $\tau_{\mathrm{VUV}} = (\sigma^2_{E\text{-THz}} - \sigma^2_E)^{0.5}/S_{\mathrm{eff}} = (15 \pm 3)$ fs for measured 1000 FLASH micropulses, where $\sigma_{E\text{-THz}}$ and σ_E are the r. m. s. widths of the krypton electron energy spectrum with and without FIR radiation.

The FIR undulator in this pump-probe experiment operates in regime of a streak camera with 10 fs resolution. The internal envelope phase stability of infrared pulse in combination with femtosecond synchronized VUV pulse permits to investigate dynamics of atomic and molecular systems with 10 fs resolution.

CONCLUSIONS

Successful operation of FEL strongly depends on the quality of the radiation detectors. XFEL MCP detectors operate in a wide dynamic range from a few nJ up to 25 mJ, and in a wide wavelength range from 0.05 to 0.4 nm for SASE1 and SASE2, and from 0.4 to 4.43 nm for SASE3. An essential feature of the detectors is high relative accuracy of measurements (below 1%), which is crucial for detection of a signature of amplification and characterization of statistical properties of the radiation. MCP detectors with these unique characteristics will be used as a key instrumentation for tuning of XFEL accelerator and searching of SASE regimes. Other diagnostic tools cannot be used for registration of XFEL radiation with so wide dynamic range and wide wavelength range. During validation tests at DORIS BW1 channel, the detector calibration was done in X-ray range at photon energies of 8.5 to 12.4 keV. At the present time the MCP detector for SASE1 was installed in XFEL tunnel, the MCP detectors for SASE2 and SASE3 will be installed in XFEL tunnel in 2016. The experimental research program with XFEL MCP detectors will start in 2017.

The far infrared undulator was designed and constructed by JINR to the FLASH. The undulator is used for longitudinal electron bunch measurements and pump-probe experiments. The measurement of undulator radiation permits to reconstruct the time distribution of the electron current in the electron bunch. The reconstructed electron current pulse has a complicated shape with two peaks at electron energy of 1.25 GeV and bunch charge 0.5 nC. The application of FIR undulator in pump-probe experiments permits to investigate dynamics of atomic and molecular systems with 10 fs resolution.

REFERENCES

1. *Syresin E. et al.* Development of MCP Based Photon Detectors for the European XFEL // IPAC11. 2011. P. 1106–1108.
2. *Brovko O. et al.* Diagnostic Technique with Femtosecond Resolution Applied for FEL Electron Bunches // RUPAC12. 2012. P. 572–574.
3. *Syresin E. et al.* Synchrotron Radiation Test Validations of European XFEL MCP Based Detectors at DORIS Beamline BW1 // IPAC14. 2014. P. 2180–2182.
4. *Syresin E. et al.* Radiation Detectors Based on Microchannel Plates for Free Electron Lasers // Phys. Part. Nucl. Lett. 2014. V. 11, No. 6. P. 730–736.
5. *Brovko O. et al.* Diagnoctics Development at JINR for ILC and FEL Ultrashort Electron Bunches // Phys. Part. Nucl. Lett. 2010. V. 7. P. 45–50.
6. *Brovko O. I. et al.* Formation and Diagnostic of Ultrashort Bunches in Free Electron Lasers // J. Appl. Phys. 2010. V. 3. P. 46–55.
7. *Brovko O. et al.* FEL Activity Developed at JINR // IPAC10, Kyoto, Japan, 2010. TUPE040. P. 2230–2232.
8. *Grimm O. et al.* Magnetic Measurements with the FLASH Infrared Undulator // Nucl. Instr. Meth. A. 2010. V. 615, No. 1. P. 105–113.
9. *Gensh M. et al.* New Infrared Undulator Beam Line at FLASH // Infrared Phys. Technol. 2008. V. 51, No. 5. P. 423–425.
10. *Frühling U. et al.* Single-Shot Terahertz-Field Driven Streak Camera // Nature Photonics. 2009. V. 3. P. 523–528.

Received on November 19, 2015.